Numerical Analysis on the Effect of n-Si on Cu(In, Ga)Se$_2$ Based Thin-Films for High-Performance Solar Cells by 1D-SCAPS

Rasika N. Mohottige*, Micheal Farndale, Gary S. Coombs, Shahnoza Saburhhojayeva

Department of Natural Sciences, Waldorf University, Forest City, IA, USA
Email: *rasika.mohottige@waldorf.edu

Abstract

We report the performances of a chalcopyrite Cu(In, Ga)Se$_2$ CIGS-based thin-film solar cell with a newly employed high conductive n-Si layer. The data analysis was performed with the help of the 1D-Solar Cell Capacitance Simulator (1D-SCAPS) software program. The new device structure is based on the CIGS layer as the absorber layer, n-Si as the high conductive layer, i-In$_2$S$_3$, and i-ZnO as the buffer and window layers, respectively. The optimum CIGS bandgap was determined first and used to simulate and analyze the cell performance throughout the experiment. This analysis revealed that the absorber layer's optimum bandgap value has to be 1.4 eV to achieve maximum efficiency of 22.57%. Subsequently, output solar cell parameters were analyzed as a function of CIGS layer thickness, defect density, and the operating temperature with an optimized n-Si layer. The newly modeled device has a p-CIGS/n-Si/In$_2$S$_3$/Al-ZnO structure. The main objective was to improve the overall cell performance while optimizing the thickness of absorber layers, defect density, bandgap, and operating temperature with the newly employed optimized n-Si layer. The increase of absorber layer thickness from 0.2 - 2 μm showed an upward trend in the cell's performance, while the increase of defect density and operating temperature showed a downward trend in solar cell performance. This study illustrates that the proposed cell structure shows higher cell performances and can be fabricated on the lab-scale and industrial levels.

Keywords

n-Si, p-CIGS, 1D-SCAPS, Thin-Films, In$_2$S$_3$

1. Introduction

Solar cells are photovoltaic (PV) devices, which directly convert light energy into

electricity. The development of solar cell applications and other renewable energy resources will be an excellent solution for the future energy crisis. Amongst available solar cells, Si-based polycrystalline devices are still dominating the photovoltaic market due to their high efficiencies and long-term stability [1]. Other types of solar cells such as thin-film, organic material, inorganic material, and dye-sensitized solar cells are currently under intense research to achieve higher efficiencies and stability [2] [3] [4]. Many researches have been devoted to improving the thin-film solar cell (second-generation solar cells) performances due to their low-cost fabrication, long-term stability, and excellent power conversion (PCE) efficiencies. Research on thin film is of great interest and with a very active research topic in the photovoltaic community, and the study of the CIGS-based solar cells is a topic under intense research. Recently worldwide research interest in cadmium telluride (CdTe) and chalcopyrite $Cu(In, Ga)Se_2$ (CIGS) based solar cells has caused considerable interest within the photovoltaic community due to their excellent PCE and cost-effectiveness. Because Cd is toxic to living beings and causes environmental concerns, investigations on CIGS-based solar cells have become more popular over CdTe-based solar cells. CIGS solar cells have shown excellent power conversion efficiencies of over 20% on lab-scale experiments [5] [6]. In addition to low cost and higher efficiencies, CIGS-based photovoltaic devices offer higher radiation resistance, durability, and lightweight, which is essential in space applications than Si-based solar cells. Therefore, CIGS has become a promising semiconductor material in the thin-film solar cell industry. Even though conventional CIGS solar cells show excellent performances, many research groups are investigating making a new device by replacing the CdS buffer layer, which produces fewer environmental concerns such as In_2S_3, ZnS, and $ZnSnO_4$, etc. Recently we have shown that n-In_2S_3 can be used as an alternative to CdS with a remarkable efficiency of 26%, which offers less health and environmental effects [7]. However, further theoretical and experimental investigations are necessary to explore CIGS-based solar cells' working principles to achieve higher efficiencies and become more popular in the photovoltaic market. Solar cells also encounter efficiency losses due to material properties and device engineering limitations like all other electronic devices. Carrier recombination is the potential drawback observed in all types of solar cells [8] [9].

Optimizing the absorber layer's physical parameters and other engineering developments will help to suppress the carrier recombination. Back-contact recombination becomes more dominant with a thinner absorber layer. Hence, the absorber layer's thickness and bandgap optimization are crucial parameters for lab-scale experiments and theoretical works to achieve better solar cell performance. In thin-film solar cell studies, p-CIGS absorber material has become more promising, because it possesses a tunable bandgap with a bandgap range of ~1.06 - 1.7 eV. One can find more details about the practical and commercial level fabrication process of CIGS-based solar cells from the available literature [10]. A conventional CIGS-based solar cell consists of Substrate/Mo/p-CIGS/

n-CdS/Al-ZnO/metal(Ni) grids. Many lab-scale and theoretical investigations have been conducted and modified in such a way as to reach different innovative ideas to achieve higher efficiencies [11]. Based on available data, most lab and commercial-based fabrications have achieved efficiencies of more than 12% [12]-[17].

To simulate realistic experimental conditions, this work extensively analyzed impacts of the absorber layer's bandgap, thickness, and defect density on output solar cell performances viz short circuit current density (J_{sc}), open-circuit voltage (V_{oc}), fill factor (FF%), power conversion efficiency (PCE) and quantum efficiency(QE%). Finally, the optimized structure was simulated by varying the operating temperature.

2. Primary Considerations for Device Simulation and Material Parameters

A deep understanding of electronic device fabrication and its working principle is vital to elevating the devices' performance and making them available at the industrial level. Implementing new device architecture, devices' engineering developments and numerical simulations provide a robust platform for that. Experimental time-scale and fabrication costs can significantly be reduced by employing numerical simulations before starting the lab-scale experiments. Hence, a large amount of theoretical research based on numerical simulations is carried out worldwide. The following sections performed a numerical simulation using one dimensional Solar Cell Capacitance Simulator (1D-SCAPS) software package (version 3.3.07) developed at the University of Gent, Belgium. Initially, SCAPS software was designed only for CdTe-based thin films. After implementing several modifications by the developers, SCAPS can now simulate Si, GaAs-based thin-film solar cells, and more details can be found in the literature [18] [19] [20] [21]. 1D-SCAPS is a powerful simulation software tool that could solve basic semiconductor equations such as Poisson's and continuity equations. Also, the SCAPS simulation can produce steady-state band diagrams, which are essential for semiconductor physics. Poisson's equation mainly describes the relationship between charge density and the electrostatic potential, and continuity equations describe the electrons and holes moving in and out of the material. These equations are given below.

$$\frac{d}{dx}\left(-\varepsilon(x)\frac{d\psi}{dx}\right) = q\left[p(x) - n(x) + N_d^+(x) - N_A^-(x) + p_t(x) - n_t(x)\right] \qquad (1)$$

$$\frac{dp_n}{dt} = G_p - \frac{p_n - p_{n0}}{\tau_p} - p_n\mu_p\frac{d\xi}{dx} - \mu_p\xi\frac{dp_n}{dx} + D_p\frac{d^2 p_n}{dx^2} \qquad (2)$$

$$\frac{dn_p}{dt} = G_n - \frac{n_p - n_{p0}}{\tau_n} + n_p\mu_n\frac{d\xi}{dx} + \mu_n\xi\frac{dn_p}{dx} + D_n\frac{d^2 n_p}{dx^2} \qquad (3)$$

where ε is the permittivity, D_p and D_n are carrier diffusion coefficients for

holes and electrons respectively, q is the electronic charge, μ is the carrier mobility, the n_p (electrons) and p_n (holes) are minority carrier concentrations, G is the generation rate, n_t and p_t are trapped electrons and holes, respectively, N_d^+ and N_A^- are ionized donors and acceptors, respectively, ψ is the electrostatic potential, and ξ is the electric field.

In the conventional CIGS cell structure, the depletion region (active region) is made with p-CIGS and the n-CdS, and the window layer is made from Al-ZnO with a bandgap of 3.30 eV. The device should have a p-n junction with a healthy depletion region to reach a better output performance. The formation of a weak depletion region will directly affect the power conversion efficiency. In this device, the n-Si layer was employed between CIGS and the buffer layer to obtain a healthy depletion region in the p-n junction and a higher conductivity in the structure. Therefore, this study proposed a new device structure with substrate/Mo/p-CIGS/n-Si/i-In$_2$S$_3$/Al-ZnO/metal grids, as depicted in Figure 1. Defect density was implemented in the CIGS, n-Si, and i-In$_2$S$_3$ layers to keep the device close to an actual device. In this study, CdS-buffer layer has been replaced by i-In$_2$S$_3$ because Cd is toxic to living beings and creates environmental concerns. Before the simulation, material parameters should be entered into software as physical input parameters. Additionally, test conditions such as operating temperature, illumination, bias voltage, etc., were set before starting the simulation. Table 1 shows the optimized and required material parameters of each layer used in this simulation.

3. Results

Robust and precise simulation software will play a vital role during new device modeling. Herein, numerical simulation was performed for a new device architecture of CIGS-based solar cell using the 1D-SCAPS simulator. The proposed structure contains a p-CIGS absorber layer, n-Si layer, and In$_2$S$_3$ as a buffer layer. In this simulation, first, each layer thickness was optimized using a pre-selected model, and 2 μm, 0.5 μm, 0.05 μm, and 0.1 μm thicknesses were selected for CIGS, n-Si, In$_2$S$_3$, and Al-ZnO layers, respectively. The CIGS layer's optimum bandgap value was determined by varying bandgap values from 1.1 eV to 1.7 eV before investigating the absorber layer thickness's impacts. Secondly, the proposed structure was investigated at various absorber layer thicknesses with the simulated optimum bandgap. In this study's final stage, the optimized cell was then simulated at multiple operating temperatures from 298 K to 400 K and various defect densities from 1.77×10^{13} to 1.77×10^{17} cm^{-3}. The incident power density was maintained at AM 1.5 (Power = 1000 Wm^{-2}).

Figure 2 depicts that efficiency increases rapidly from 1.1 eV to 1.4 eV, then remains constant until 1.7eV. Therefore, it is apparent that a thin-film solar cell's efficiency significantly depends on the selected semiconductor material's bandgap. This work used 1.4 eV as the CIGS layer's optimized bandgap throughout the experiment based on the simulation.
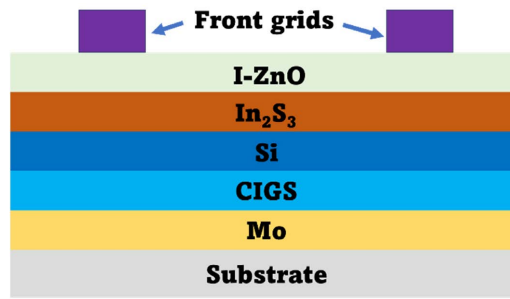
Figure 1. Schematic diagram of proposed structure.

Table 1. Optimized material parameters used in the simulation.

| Parameters	p-CIGS	n-Si	i-In$_2$S$_3$	Al-ZnO
Thickness (μm)	0.2 - 2	0.5	0.05	0.1
Bandgap (eV)	1.4	1.12	2.8	3.3
Electron affinity (eV)	4.5	4.0	4.7	4.5
Relative permittivity	13.6	9.8	13.5	9.0
CB (1/cm^3)	2.2×10^{18}	2.8×10^{19}	1.8×10^{18}	2.2×10^{18}
VB (1/cm^3)	1.8×10^{19}	2.65×10^{19}	4.0×10^{13}	1.8×10^{19}
Electron mobility (cm^2/Vs)	100	100	400	100
Hole mobility (cm^2/Vs)	25	100	210	25
ND (1/cm^3)	0	1.0×10^{20}	1.0×10^{5}	1.0×10^{18}
NA (1/cm^3)	2.0×10^{16}	0	10	0
Defects density (1/cm^3)	1×10^{13} - 1×10^{17}	1×10^{14}	1×10^{14}	0
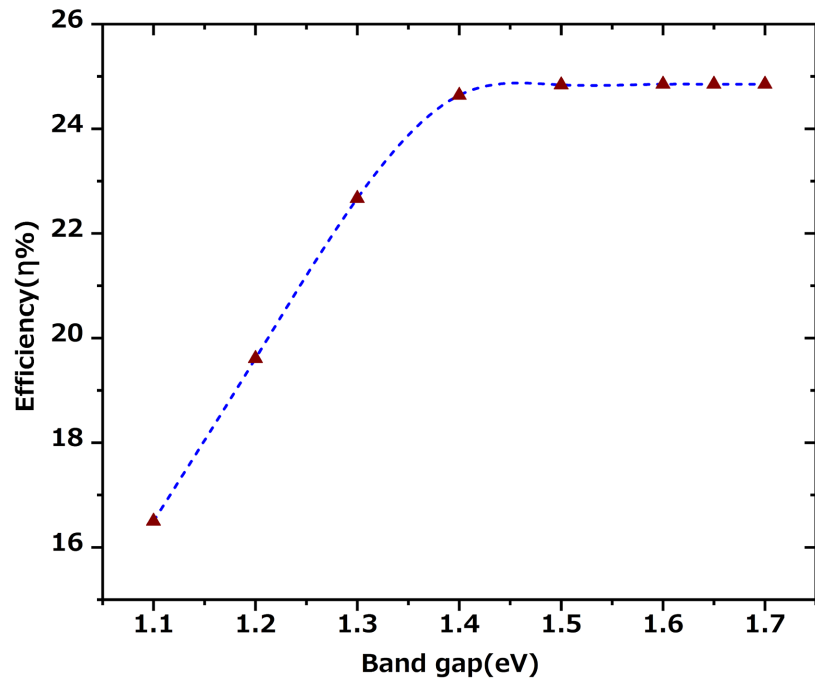
Figure 2. Efficiency variation as a function CIGS bandgap.

After optimizing the CIGS absorber layer's bandgap, thickness has been numerically investigated in the ranges of 0.2 μm to 2 μm while keeping other material parameters of different layers constant. This study's main objective was to optimize the absorber layer thickness to achieve maximum output performance with minimal cell's power conversion efficiency (PCE) losses. A heterojunction solar cell is essentially a p-n junction device. Therefore, it is crucial to confirm the formation of the p-n junction in the thin-film structure.

The energy band diagram (EBD) is the most evident signature of the thin film's p-n junction building. **Figure 3** presents the energy band diagram of the CIGS-based cell structure of this study. The energy band diagram shows different recombination regions named A, B, C & D. Regions A & B are assigned to recombination at back contact and bulk recombination. Thus the energy band diagram confirms that by increasing absorber layer thickness, back contact recombination current density significantly reduces and ensures the enhancement of cell output performances. Also, the formation of region C (depletion layer) in EBD confirms that the proposed structure has a healthy, active region essential for higher performance.

Solar cell output performances, viz V_{oc}, J_{sc}, FF, and PCE, are shown in **Figure 4**, and the simulation results are summarized in **Table 2**. The results clearly show that J_{sc}, V_{oc}, FF, and PCE have increased as the absorber layer's thickness increases. The maximum efficiency value of 22.57% was achieved at 2 μm. The rapid rise in output parameters, V_{oc}, J_{sc}, FF & PCE, can be observed in the thickness ranging from 0.2 μm to 0.8 μm, and 0.8 μm to 2 μm will only increase slightly, which means saturation phase has been reached. Thickness optimization of the absorber and the buffer layer is essential for an efficient photovoltaic
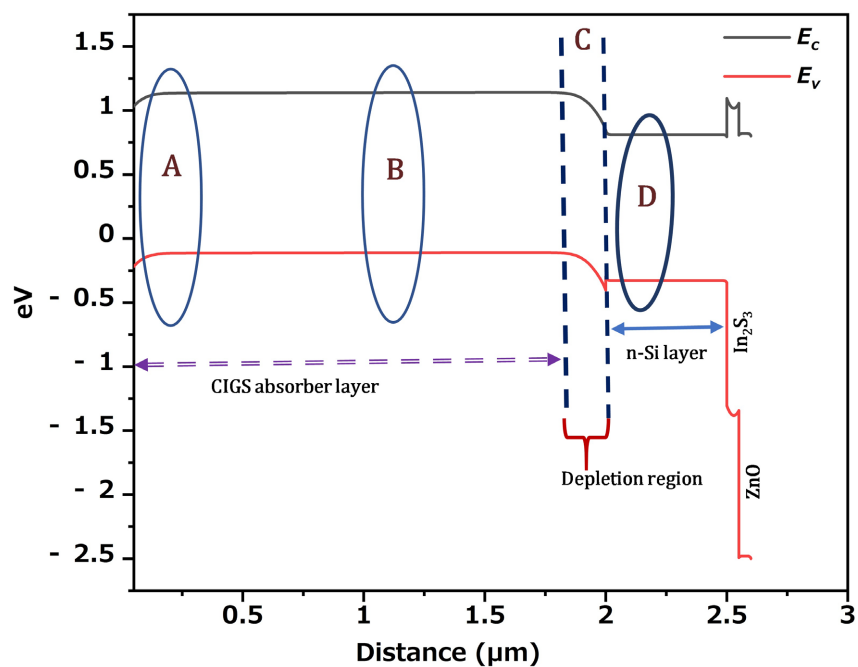

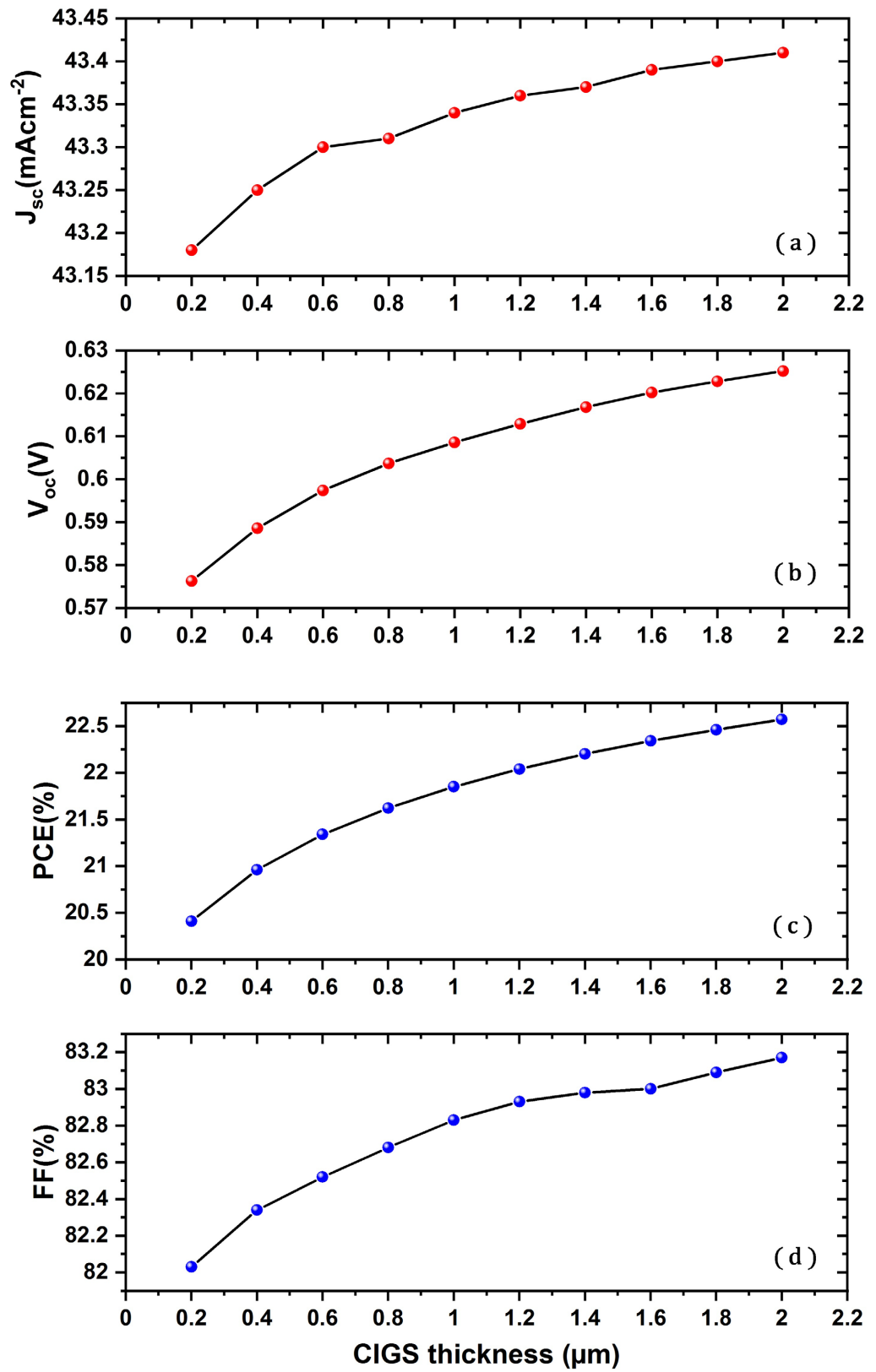**Figure 3.** Energy band diagram of proposed structure.

Figure 4. Solar cell's output performance enhancement as a function of CIGS absorber layer thickness (a) Short circuit current density, (J_{sc}) (b) Open circuit voltage (V_{oc}), (c) Power conversion efficiency (PCE), (d) Fill factor (FF).

Table 2. Solar cell performance as a function of the CIGS layer thickness.

CIGS thickness (µm)	V_{oc} (V)	J_{sc} (mA/cm^2)	FF (%)	PCE (%)
0.2	0.5763	43.18	82.03	20.41
0.4	0.5886	43.25	82.34	20.96
0.6	0.5974	43.28	82.52	21.34
0.8	0.6037	43.31	82.68	21.62
1.0	0.6086	43.33	82.83	21.85
1.2	0.6129	43.35	82.93	22.04
1.4	0.6168	43.37	82.98	22.20
1.6	0.6202	43.38	83.00	22.34
1.8	0.6228	43.39	83.09	22.46
2.0	0.6252	43.40	83.17	22.57

device. Recently we have shown that the In_2S_3 buffer layer is a promising and robust alternative for CdS. Also, buffer layer thickness variation from 20 nm to 100 nm had a minimum effect on the cell's performance [22]. Thus the extensive investigation of how In_2S_3 buffer layer thickness impacts the output performance has been excluded from this study.

It is evident that CIGS layer thickness is directly proportional to the number of absorbed photons, contributing to generating more electron-hole pairs (e-h) before recombination with the back contact and, consequently, enhancing the cell's overall efficiency. According to Figure 5, back contact recombination is drastically reduced, while in Figure 6, bulk recombination current density increases as the absorber layer's thickness increases.

However, obtaining higher CIGS absorber layer thickness is still challenging because of the high fabrication cost during mass production due to the high indium content (In) and gallium (Ga). Hence, it was evident from the results that the optimum absorber layer thickness should be around 2 µm to minimize the material consumption without any significant impact on solar cell efficiency. Also, cells with thinner absorber layers will negatively affect the cell's performance by increasing back-contact recombination. Because the back contact is located near the depletion region of the p-n junction, this will cause higher recombination with the back contact and result in a downward trend in output performance. Therefore, more experimental research needs to be performed to determine the CIGS absorber layer's optimum thickness to obtain higher efficiencies. Output performances of photovoltaic devices are highly dependent on the spectrum of the incident light. Hence, the proposed device was studied within the spectral range of 300 nm (4.13 eV) - 1200 nm (1.03 eV). The spectral response of the device is measured in terms of quantum efficiency (QE%). QE (λ) of a photoactive material is the number of carriers measured at the output detector per number of incident photons per unit time. It estimates the device's ability to convert a photon flux to a photogenerated electric current and can be expressed by Equation (4).
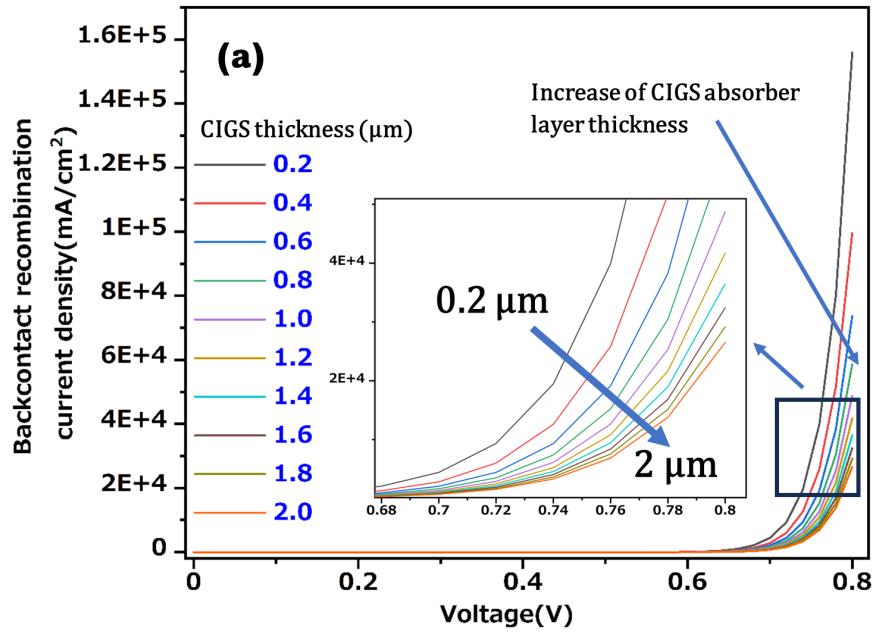
Figure 5. Variation of back contact recombination current density.
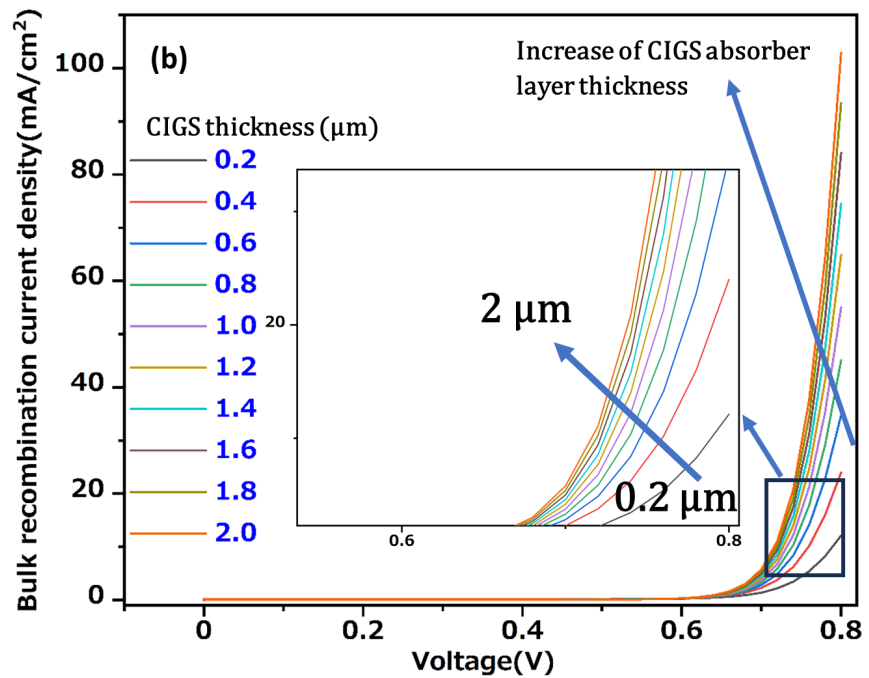

Figure 6. Bulk recombination current density due the increase of CIGS layer thickness.

$$\text{QE}(\lambda) = \frac{J_{ph}}{q\phi} \qquad (4)$$

where J_{ph} is the photogenerated current density, q is the electronic charge, and ϕ is the number of incident photons.

The thickness of the absorber layer affected the QE% of the cell, and **Figure 6** shows the variation of QE% under AM 1.5 as a function of CIGS absorber layer

thickness. As expected, by increasing CIGS layer thickness, many photons are absorbed towards the higher thickness range, resulting in more photogenerated carriers collected before recombination and directly enhancing the QE%. There are three distinct regions in **Figure 6**; above 600 nm, 440 nm to 520 nm, and below 400 nm. Above 600 nm, one can observe that QE% has progressively increased from 0.2 - 2 μm due to the spectrum's high absorption by thicker layers, thus lowering the recombination, ensuring the maximum QE%. Nevertheless, below 400 nm, one can observe the blue response mainly due to front surface recombination. The change in QE% from 440 nm to 520 nm is apparent in **Figure 7** due to the buffer layer's influence.

However, the defect density of polycrystalline material significantly affected the performance of the cell. It is well known that defects in the absorber layer influence the device output solar cell parameters. Hence, to get a deep understanding of defect density in the absorber layer, PCE and FF parameters were simulated. Meanwhile, the defect density was changed from 1.77×10^{13} to 1.77×10^{17} cm^{-3}. The effects of defect density on PCE & FF% are shown in **Figure 8**. As the defect density increases, PCE decreases from 22.17% to 10.57%, and FF% decreases from 84.30 to 69.35 which means defects at the absorber layer in the cell are unfavorable for the efficiency fill factor. This observation can be attributed to higher defect density leading to a higher recombination rate, which reduces the cell's efficiency.

4. Discussion

4.1. Impact of CIGS Layer Thickness on V_{oc}, J_{sc}, FF, PCE, and QE%

Many numerical simulation studies have been conducted on conventional thin-film
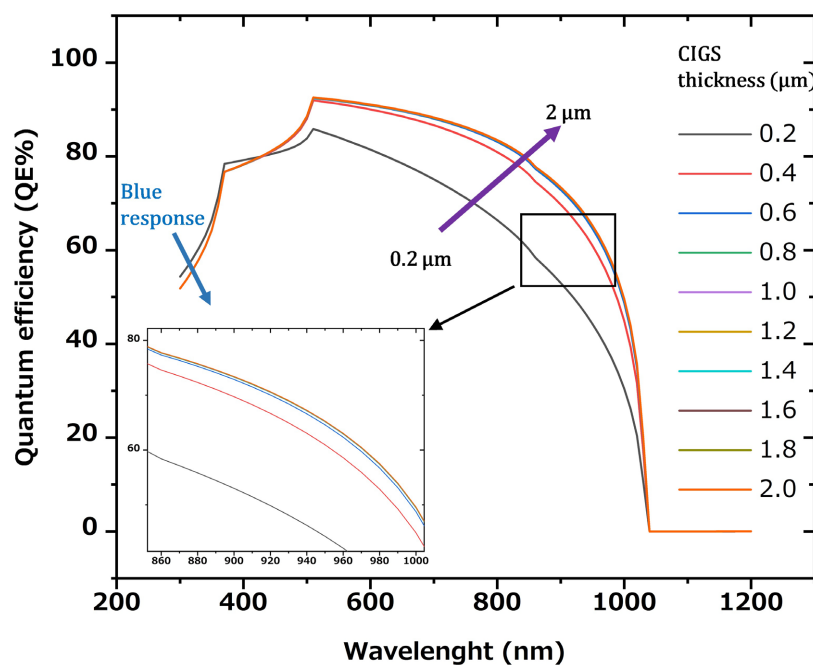

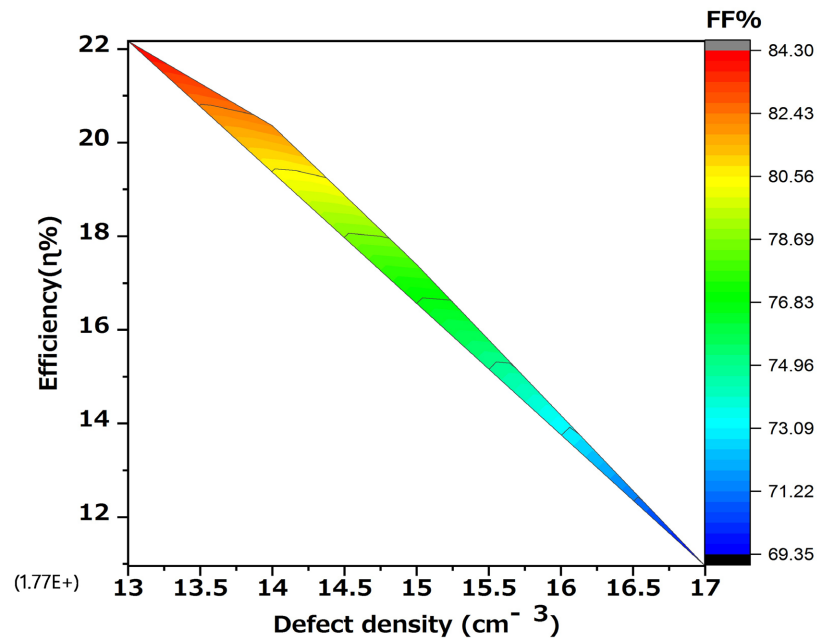**Figure 7.** Effect of CIGS thickness on the quantum efficiency (QE%).

Figure 8. Variation of efficiency & fill factor with absorber layers' defect density.

CIGS-based solar cells. Hence, this study determined the cell's output performance with the n-Si layer for the first time. As mentioned in the previous section, the impact of the thickness variation was studied only for the absorber layer, and thicknesses of other layers were kept at standard optimized values. CIGS absorber is the most crucial layer in the thin-film structure. It is a chalcopyrite semiconductor material with a bandgap in the range of 1.06 eV - 1.7 eV. Therefore, before investigating the thickness, defect density, and temperature effect on the cell's performance, it is vital to research the absorber layer's optimum bandgap, which corresponds to the maximum efficiency. At first, the CIGS layer's optimum bandgap value was simulated and determined in the range of minimum and maximum bandgap values of 1.1 to 1.7 eV, respectively.

4.2. Impact of Operating Temperature on V_{oc}, J_{sc}, FF, PCE, and QE%

All kinds of solar cells are highly responsive to operating temperature, and the temperature variations directly affect the cell's performance. Hence, the operating temperature becomes a vital physical parameter to investigate when modeling and using lab-scale fabrications. Solar cells should work with a minimum performance loss within the considerable temperature range. CIGS-based solar cells are specially designed for outdoor applications and space applications due to their stability in the temperature range of 59°F to 122°F. The open-circuit voltage (V_{oc}), short circuit current density (J_{sc}), fill factor (FF), QE%, and power conversion efficiency (η%) are temperature-dependent parameters. V_{oc} is the most vulnerable output solar cell parameter affected by operating temperature. As depicted in **Figure 9**, V_{oc} decreases linearly as the temperature increases. Saturation current density (J_0) controls the V_{oc}, and J_0 is highly sensitive to operating temperature. The following equation shows the relationship between J_0 and V_{oc}.
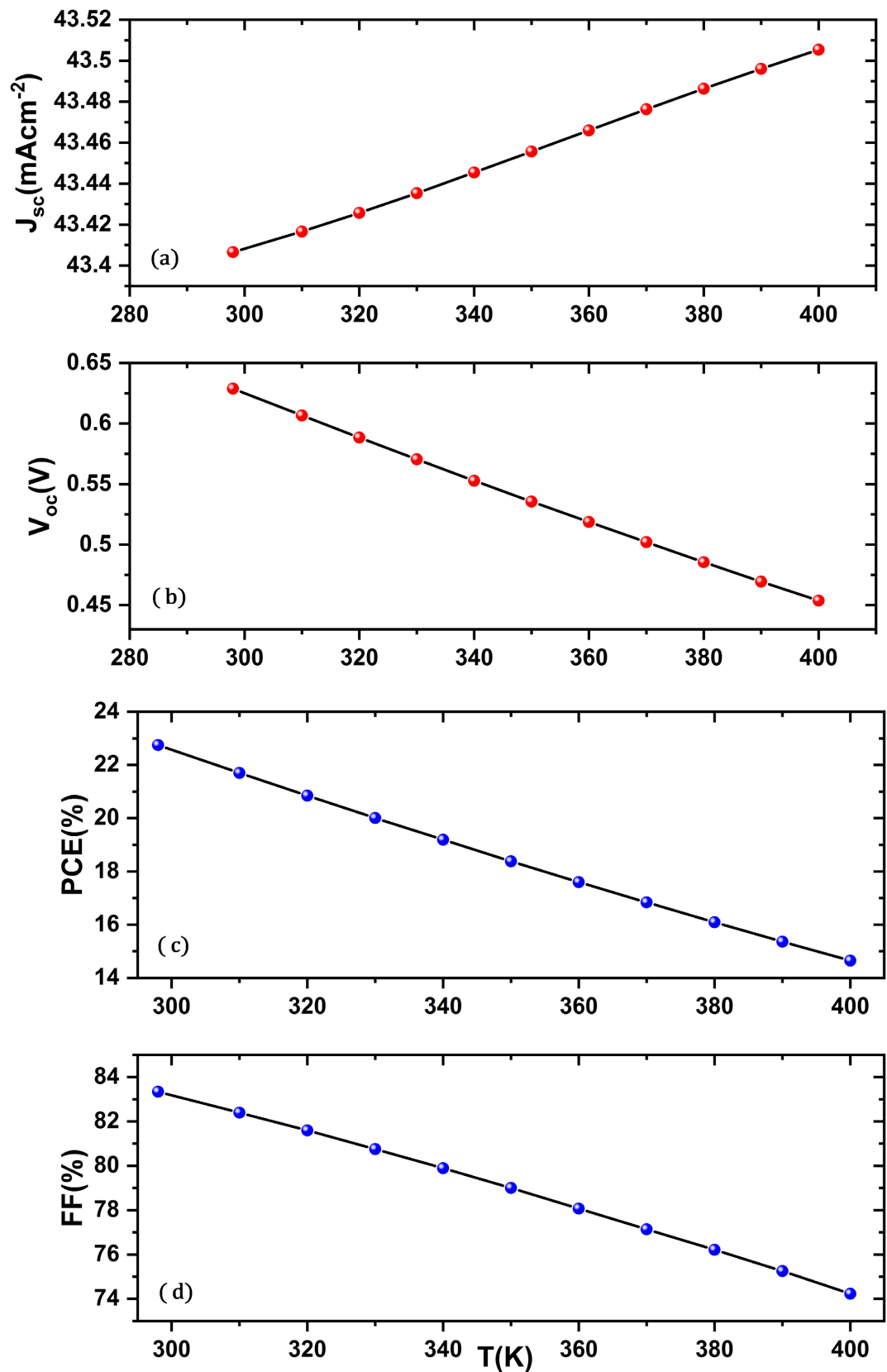
Figure 9. Solar cell's output performance as a function of operating temperature (a) Short circuit current density (*J*sc), (b) Open circuit voltage (*V*oc), (c) Power conversion efficiency (PCE), (d) Fill factor (FF).

$$V_{oc} = \frac{kT}{q} \ln\left(\frac{J_{sc}}{J_0} + 1\right) \qquad (5)$$

where k = the Boltzmann constant and q = the electronic charge.

All semiconductor devices are susceptible to temperature. An increase in temperature reduces the semiconductor material's bandgap, negatively impacting most of the semiconductor devices' performances. This is because high-energy electrons in the conduction band lower the binding energy and reduce bandgap energy at higher temperatures. This leads to increasing J_{sc} because more photons

Table 3. Solar cell performance at various temperatures.

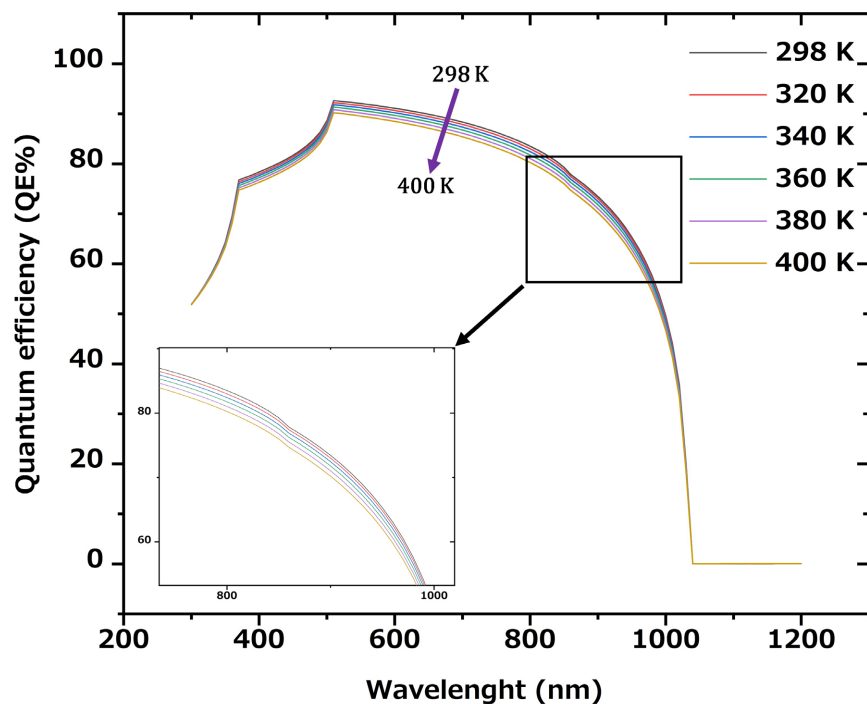| Temperature (K)	V_{oc} (V)	J_{sc} (mA/cm^2)	FF (%)	PCE (%)
298	0.6288	43.40	83.34	22.75
310	0.6066	43.41	82.39	21.70
320	0.5884	43.42	81.59	20.85
330	0.5704	43.43	80.75	20.01
340	0.5528	43.44	79.89	19.19
350	0.5355	43.45	79.00	18.38
360	0.5187	43.46	78.07	17.60
370	0.5020	43.47	77.14	16.84
380	0.4855	43.48	76.21	16.09
390	0.4694	43.49	75.25	15.36
400	0.4537	43.51	74.23	14.65

Figure 10. Quantum efficiency of the cell at different operating temperatures.

are involved in creating more electron-hole pairs (e-h). But at high temperatures, FF and PCE have shown a downward trend. As expected from Equation (4), Figure 10 further proves the downward trend in QE% as the operating temperature increases. Table 3 shows the operating temperature dependence values for J_{sc}, V_{oc}, FF%, and PCE.

5. Conclusion

In summary, this novel study shows that n-Si is an excellent candidate to build a pn junction with a healthy depletion layer. Furthermore, it was found out that the CIGS layer's optimum bandgap energy was 1.4 eV and the optimized thickness was 2 μm. Thickness optimization of the absorber layer is vital to reduce material consumption and consequently relieve the fabrication cost. Additionally, at higher operating temperatures (above 310 K) and higher defect densities (above 1.77×10^{13}) in the absorber layer, the optimized cell shows a downward trend in power conversion efficiency; however, further lab-scale experiments are needed to implement the outcome of this simulation work.

Acknowledgements

Conflicts of Interest

The authors declare no conflicts of interest regarding the publication of this paper.

References

[1] Wolden, C.A., *et al.* (2011) Photovoltaic Manufacturing: Present Status, Future Prospects, and Research Needs. *Journal of Vacuum Science & Technology A*, **29**, Article ID: 030801. https://doi.org/10.1116/1.3569757

[2] Chopra, K.L., Paulson, P.D. and Dutta, V. (2004) Thin-Film Solar Cells: An Overview. *Progress in Photovoltaics: Research and Applications*, **12**, 69-92. https://doi.org/10.1002/pip.541

[3] Grätzel, M. (2001) Photoelectrochemical Cells. *Nature*, **414**, 338-344. https://doi.org/10.1038/35104607

[4] Bernede, J.C. (2008) Organic Photovoltaic Cells: History, Principle, and Techniques. *Journal of the Chilean Chemical Society*, **53**, 1549-1564. https://doi.org/10.4067/S0717-97072008000300001

[5] Green, M.A., Emery, K., Hishikawa, Y., Warta, W. and Dunlop, E.D. (2013) Solar Cell Efficiency Tables (Version 41). *Progress in Photovoltaics: Research and Applications*, **21**, 1-11. https://doi.org/10.1002/pip.2352

[6] Jackson, P., *et al.* (2011) New World Record Efficiency for Cu(In,Ga)Se₂ Thin-Film Solar Cells beyond 20%. *Progress in Photovoltaics: Research and Applications*, **19**, 894-897. https://doi.org/10.1002/pip.1078

[7] Shockley, W. (1961) Problems Related to P-N Junctions in Silicon. *Solid-State Electron*, **2**, 35-60. https://doi.org/10.1016/0038-1101(61)90054-5

[8] Pudov, A., Sites, J. and Nakada, T. (2002) Performance and Loss Analyses of High-Efficiency Chemical Bath Deposition (CBD)-ZnS/Cu(In$_{1-x}$Ga$_x$)Se$_2$ Thin-Film Solar Cells. *Japanese Journal of Applied Physics*, **41**, L672. https://doi.org/10.1143/JJAP.41.L672

[9] Kosyachenko, L.A., Mathew, X., Paulson, P.D., Lytvynenko, V.Y. and Maslyanchuk, O.L. (2014) Optical and Recombination Losses in Thin-Film Cu(In,Ga)Se$_2$ Solar Cells. *Solar Energy Materials and Solar Cells*, **130**, 291-302. https://doi.org/10.1016/j.solmat.2014.07.019

[10] Micheal, P., *et al.* (2017) Advances in Cost-Efficient Thin-Film Photovoltaics Based on Cu(In,Ga)Se$_2$. *Engineering*, **3**, 445-451. https://doi.org/10.1016/J.ENG.2017.04.015

[11] Vermang, B., *et al.* (2013) Development of Rear Surface Passivated Cu(In,Ga)Se$_2$ Thin Film Solar Cells with Nano-Sized Local Rear Point Contacts. *Solar Energy Materials and Solar Cells*, **117**, 505-511. https://doi.org/10.1016/j.solmat.2013.07.025

[12] Dharmadasa, I.M. (2009) Fermi Level Pinning and Effects on Cu(In,Ga)Se$_2$-Based Thin-Film Solar Cells. *Semiconductor Science and Technology*, **24**, Article ID: 055016. https://doi.org/10.1088/0268-1242/24/5/055016

[13] Vaynzo, Y., Bakulin, A.A., Gélinas, S., *et al.* (2012) Direct Observation of Photoinduced Bound Charge-Pair States at an Organic-Inorganic Semiconductor Interface. *Physical Review Letters*, **108**, Article ID: 246605. https://doi.org/10.1103/PhysRevLett.108.246605

[14] Zhang, S.B., Wei, S.H. and Zunger, A. (1997) Stabilization of Ternary Compounds via Ordered Arrays of Defect Pairs. *Physical Review Letters*, **78**, 4059-4062. https://doi.org/10.1103/PhysRevLett.78.4059

[15] Zhang, S.B., Wei, S.H. and Zunger, A. (1998) Defect Physics of the CuInSe$_2$ Chalcopyrite Semiconductor. *Physical Review B*, **57**, 9642-9656. https://doi.org/10.1103/PhysRevB.57.9642

[16] Sugiyama, M., Nakai, R., Nakanishi, H., *et al.* (2003) Interface Fermi Level Pinning in a Cu/P-CuGaS$_2$ Schottky Diode. *Journal of Physics and Chemistry of Solids*, **64**, 1787-1790. https://doi.org/10.1016/S0022-3697(03)00144-6

[17] Dharmadasa, I.M., Bunning, J.D., Samantilleke, A.P., *et al.* (2005) Effects of Multi-Defects Metal/Semiconductor Interfaces on Electrical Properties and Their Influence on Stability and Life Time of Thin Film Solar Cells. *Solar Energy Materials and Solar Cells*, **86**, 373-384. https://doi.org/10.1016/j.solmat.2004.08.009

[18] Heriche, H., *et al.* (2017) New Ultra-Thin CIGS Structure Solar Cells Using SCAPS Simulation Program. *International Journal of Hydrogen Energy*, **42**, 9524-9532.

[19] Mostefaoui, M., Mazan, H., Khelifi, S., Bouraiou, A. and Dabou, R. (2015) Simulation of High Efficiency CIGS Solar Cells with SCAPS-1D Software. *Energy Procedia*, **74**, 736-744. https://doi.org/10.1016/j.egypro.2015.07.809

[20] Burgelman, M., Nollet, P. and Degrave, S. (2000) Modelling Polycrystalline Semiconductor Solar Cells. *Thin Solid Films*, **361**-**362**, 527-532. https://doi.org/10.1016/S0040-6090(99)00825-1

[21] Burgelman, M. and Marlein, J. (2008) Analysis of Graded Bandgap Solar Cells with SCAPS. *Proceedings of the* 23*rd European Photovoltaic Solar Energy Conference*, Valencia, 1-5 September 2008, 2151-2155.

[22] Mohottige, R.N. and Vithanage, S.P.K. (2021) Numerical Simulation of a New Device Architecture for CIGS-Based Thin-Film Solar Cells Using 1D-SCAPS Simulator. *Journal of Photochemistry and Photobiology A: Chemistry*, **407**, Article ID: 113079. https://doi.org/10.1016/j.jphotochem.2020.113079